Analysis of Cell Flux in the Parallel Plate Flow Chamber: Implications for Cell Capture Studies

Lance L. Munn, Robert J. Melder, and Rakesh K. Jain

Department of Radiation Oncology, Harvard Medical School and Massachusetts General Hospital, Boston, Massachusetts 02114 USA

ABSTRACT   The parallel plate flow chamber provides a controlled environment for determinations of the shear stress at which cells in suspension can bind to endothelial cell monolayers. By decreasing the flow rate of cell-containing media over the monolayer and assessing the number of cells bound at each wall shear stress, the relationship between shear force and binding efficiency can be determined. The rate of binding should depend on the delivery of cells to the surface as well as the intrinsic cell-surface interactions; thus, only if the cell flux to the surface is known can the resulting binding curves be interpreted correctly. We present the development and validation of a mathematical model based on the sedimentation rate and velocity profile in the chamber for the delivery of cells from a flowing suspension to the chamber surface. Our results show that the flux depends on the bulk cell concentration, the distance from the entrance point, and the flow rate of the cell-containing medium. The model was then used in a normalization procedure for experiments in which T cells attach to TNF-α-stimulated HUVEC monolayers, showing that a threshold for adhesion occurs at a shear stress of about 3 dyn/cm^2.

INTRODUCTION

The parallel plate flow chamber (Fig. 1) allows the study of cellular binding in a well defined shear field, and many investigators have used this device to measure the wall shear stress at which adherent cells detach from the surface. In these studies, cells are incubated under stagnant conditions on a microscope slide coated with a protein or a cell monolayer that constitutes the bottom surface of the flow chamber, and cell-free media is then perfused through the device in an attempt to dislodge the cells from the surface (Hochmuth et al., 1972; Gallik et al., 1989; Abassi et al., 1991; van Kooten et al., 1992).

Another use for the parallel plate flow chamber is in the evaluation of the range of wall shear stresses at which cell capture occurs, as described by Doroszewski et al. (1979). The mechanics of cell capture are quite different from the mechanics of cell detachment because of strengthening mechanisms that function after stable adhesion is attained (Mege et al., 1986). Mechanisms of adhesion reinforcement include the spreading of cells on the substrate as well as the recruitment of receptors to the area of contact (which may be independent of cell spreading). Studies of capture shear stresses can identify the contributions of the various adhesion molecules involved in cell attachment to the endothelium and provide a better understanding of cell delivery in vivo. In cell detachment assays, on the other hand, the roles of the individual adhesion pathways can be obscured because of these strengthening mechanisms.

A convenient approach to studying binding kinetics over a wide range of shear rates involves initiating the flow of cell suspension at a high rate and then decreasing the flow in a step-wise fashion until appreciable cell binding occurs. The number of cells that bind at each flow rate is inevitably dependent on the number of cells near the surface available for binding, and the question, therefore, becomes one of binding kinetics versus collision frequency. Forrester and Lackie (1984) introduced a normalization procedure in an attempt to account for the contribution of cell flux to the binding rate. They defined a "collection efficiency" by dividing the number of bound cells by the total number of cells that pass through the chamber. The implicit assumption in this normalization is that the concentration of cells at the surface is the same as that in the bulk.

We propose that a more appropriate indication of collision rate between cells in suspension and the chamber surface is the flux based on the local cell concentration near that surface. Careful review of videotaped experiments at various flow rates shows that the concentration of cells near the surface varies with the flow rate and with the distance from the entrance point. For cell binding experiments, it is necessary, therefore, to characterize the delivery of cells to the bottom surface of the chamber in terms of the flow rates and spatial coordinates, and to use this local concentration in a normalization procedure.

Calculation of the actual collision frequency between the flowing cells and the surface is a formidable task and, indeed, the behavior of the cells as they approach the surface appears unpredictable. This can be attributed to 1) van der Waals and other molecular forces that come into play as the cells come into close proximity, and/or 2) complex fluid dynamics in this region. Even with a relatively smooth, spherical structure such as a liposome, Wattenbarger et al. (1990) found that the behavior very close a glass substrate deviated from their model's predictions. Now consider a surface coated with an endothelial monolayer, with an uneven surface topology. The regions above the nuclei protrude approximately 2–3 μm above the surface, whereas the intercellular regions have a

height of a fraction of a micrometer. This surface morphology causes variations in the fluid dynamics close to the surface and, hence, perturbations in the cell trajectory. This can be seen as the cells pass by the layer in the region considered in the analysis—they tend to swerve and dip as they encounter the "peaks and valleys" on the surface.

In addition, microvilli on the passing cell can protrude over distances on the order of a micron from the surface, extending the cell's range of grasp to much greater than 20–50 nm, which is the generally accepted binding distance. These surface features would also be expected to alter the trajectory of the cells through the fluid. Because of these complications in the cell behavior as they near the surface, we do not attempt to calculate collision frequencies, but instead implement a first-order correction for the varying surface fluxes caused by sedimentation.

The analysis considers a volume element of fluid with height h above the chamber surface (Fig. 2), defined by the depth of field of the microscope objective used in the experimental observations. Cells accumulate in this thin layer directly above the surface because of 1) cells that contact the surface but do not achieve stable adhesion and, therefore, flow near the surface until a successful interaction is achieved and 2) the sharp decrease in sedimentation velocity as cells approach a surface. This results in a local concentration near the surface that is higher than the bulk cell concentration.

The analysis is based on the sedimentation of cells in the chamber. Wattenbarger et al. (1990) used a similar rationale in a detailed study of liposome trajectories in the flow cell. This work, however, was concerned with the approach and interactions of individual liposomes at the surface, whereas we are interested in the total flux of cells at a particular location at a given flow rate. An analysis of the rates of settling and the velocities of cells along the chamber shows that the local cell concentration depends on both the flow rate and spatial coordinate, and provides a convenient method for normalizing the cell binding data.
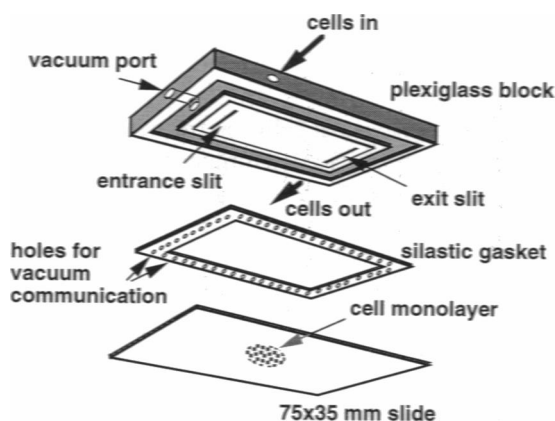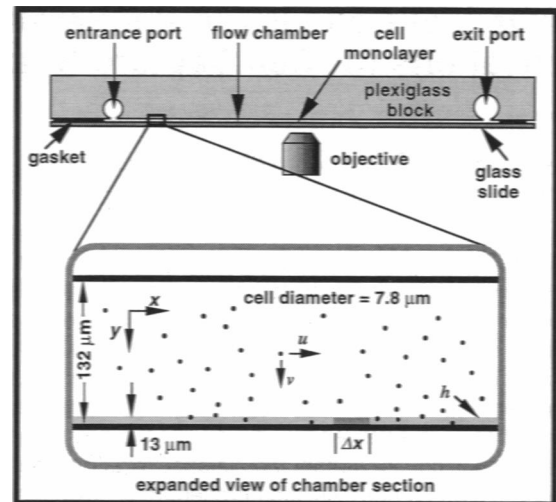

FIGURE 2 The parallel plate flow chamber apparatus in cross section and an expanded view of the flow chamber region. h defines a 13-μm layer of fluid at the bottom of the chamber. The cell monolayer occupies approximately 1 cm² at the center of the bottom surface.

MATERIALS AND METHODS

Normal human T lymphocytes were isolated from buffy coat preparations diluted 1:1 with Hanks balanced salt solution (HBSS) and centrifuged over a Histopaque gradient (Sigma Chemical Co., St. Louis, MO). The lymphocyte layer was then depleted of monocytes by incubation with PME (L-phenylalanine methyl ester, E.I. du Pont de Nemours, Wilmington, DE) for 15 minutes (Leung, 1989). The T lymphocytes were isolated according to a modified method of antibody-mediated cell depletion using anti-CD19, CD16, and CD15 antibodies (Yaumachi and Bloom, 1993). In cell binding experiments, T cells at 10⁶/ml were perfused over a TNF-α (tumor necrosis factor-α, Cetus, Emeryville, CA; 50 ng/0.3 ml at 37°C for 5 h) activated HUVEC (human umbilical vein endothelial cell) monolayer at the bottom of the parallel plate flow chamber. A computer-driven variable speed syringe pump (Harvard Apparatus, South Natick, MA) pulled cells suspended in HBSS from a reservoir through the chamber. An IBM PC controlled the operation of the pump and prompted the operator to position the stage for five acquired fields at each flow rate. The flow rate was decreased from 2 ml/min (4.1 dyn/cm² wall shear stress) to 0.2 ml/min (0.41 dyn/cm²) in steps of 0.2 ml/min. Five fields were sampled at each flow rate, and the images were recorded on a video cassette for later analysis.

Analyses of cell concentration near the surface and cell velocities were performed without a HUVEC monolayer. The number of cells within the 13 μm depth of field of the microscope was determined at various flow rates and locations in the chamber by image analysis. Fig. 2 illustrates the flow chamber apparatus and an expanded view of the chamber cross section. The channel width is 2.5 cm and the length is 6 cm. The height h was defined by the depth of field of the 0.25 NA 10x objective used for the experimental observations. With phase contrast optics, the cells appeared as bright objects on a dark field, and cells that were within the layer h were easily distinguished from cells farther from the surface. The total optical magnification was 60x, and the field of view (480x325 μm) covered approximately 0.16 mm² of the surface.

In the cell binding experiments, the objective was maintained at 2.75 cm from the entrance slit (i.e., at the center of the chamber), and sampling was only performed along the width of the chamber. The time between flow rate steps was adjusted so that the total number of cells passing over the layer at each step was the same (see Results and Discussion). The number of cells bound at each flow rate was determined by image analysis of the video taped experiments. A cell was defined as bound if it did not detach or roll during the 5 s sampling time.

FIGURE 1 Schematic of the parallel plate flow chamber. The apparatus is held together by vacuum, forming a constant gap width of 132 mm between the upper surface and the microscope slide.

THEORY

Cell sedimentation rate and velocity near the wall

In the analysis of cell delivery to the surface, the cell velocities in the x and y directions are considered separately. The decrease of the x component of the velocity for spheres flowing parallel to a surface described by Goldman et al. (1967) was used in the calculation of the average translational velocity of the cells. The theory strictly applies to neutrally buoyant spheres translating in Couette flow, but near the wall the parabolic profile is approximately linear and the flow can be assumed to be Couette. Because we are only concerned with the bulk behavior of the cells in the region h, we can obtain an average effective velocity for the cells in this region by integrating over the nonlinear correction function. This yields an average velocity for cells moving within h along the flow chamber of $0.117\,Q$ (cm/s, with the flow rate Q in ml/min). This is a factor of 0.84 slower than the uncorrected average velocity in h.

The presence of the flow chamber surfaces (top and bottom plate) also affects the sedimentation rates of the cells. Brenner (1961) studied the effect of solid surfaces in slowing the sedimentation of rigid spheres and derived the appropriate correction for the Stokes sedimentation law. Taking into account the contributions of both the top and bottom surfaces of the chamber, the corrected average sedimentation velocity in the region above h is slower than the Stokes velocity for free sedimentation by a factor of 0.86.

To determine the time and position dependencies of the cell flux at the surface, we perform a balance on the cell concentration Ψ (cells·cm^{-3}) in a volume element within the layer h (Fig. 2). Cells enter the volume element from above at rate Cv (cells·cm^{-2}·s^{-1}) because of settling and from the left because of the bulk motion of the stream with velocity u(cm·s^{-1}). C is the bulk concentration, v is the average settling velocity for cells above h, and u is the average cell velocity in the x direction within h. Cells exit the element with the bulk flow at $x + \Delta x$ and by binding to the surface with rate R (cells·cm^{-2}·s^{-1}).

The supply of cells from the bulk solution is independent of the x position. A pulse of cells injected into the chamber will distribute in a nonuniform manner on the bottom surface of the chamber (Fig. 3), but for continuous flow of cells into the chamber, the increase in flux caused by a higher velocity at the center of the inlet exactly balances the spreading effect. In other words, the divergence of the streamlines at the surface in the x direction caused by the parabolic flow profile is countered by the variation in flux at the entrance that is also caused by this parabolic profile.

This can be shown as follows. Neglecting the small effect of the walls in the region above h, the trajectory of a cell through the chamber starting at y_0 (where y is measured from the center of the chamber height) is given by

$$x = \frac{Q}{4vb^3w}[3b^2(y_0 - y) + y^3 - y_0^3] \qquad (1)$$

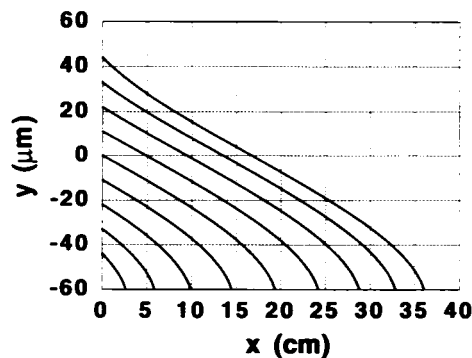where Q is the flow rate, b is the chamber half-height, v is

FIGURE 3　Cell trajectories in the bulk fluid for various entrance heights. The flow rate for all curves is 1 ml/min.

the constant sedimentation velocity, and w is the chamber width. This expression was derived by combining the parabolic translational velocity profile with a constant sedimentation velocity in the y direction. The trajectories for a number of starting positions are shown in Fig. 3.

Now consider the cell flux at the entrance and the fate of these cells in the region just above h. A simple balance on the fluxes contained between any two trajectories gives

$$u(y_0)C\Delta y_0 = vC_b\Delta x \qquad (2)$$

where $u(y_0)$ is the velocity in the x direction at $x = 0$, C_b is the concentration at $y = -b$, and C is the bulk (entrance) concentration. Δy_0 is the vertical height of the entrance flux being considered (the differential distance at $x = 0$), and Δx is the corresponding length at $y = -b$. This gives the condition

$$\frac{dx}{dy_0} = \frac{u(y_0)C}{vC_b}. \qquad (3)$$

Substitution of the derivative from Eq. 1 and the parabolic velocity profile for $u(y_0)$ yields $C_b = C$; the concentration does not deviate from the bulk concentration along the chamber. Because the sedimentation velocity is constant, the sedimentation flux is invariant with position.

For the analysis of flux near the surface, we consider the bulk behavior of the cells in the region h, and neglect any variation of the concentration in the y direction within this control volume. A balance on the fluxes yields the partial differential equation for the cell concentration Ψ within h:

$$\frac{\partial\Psi}{\partial t} = \frac{Cv - R}{h} - u\frac{\partial\Psi}{\partial x} \qquad (4)$$

where R is the rate of binding to the surface. In general, the rate of binding is much less than the rate of delivery, so R can be neglected compared to Cv. At steady state $(\partial\Psi/\partial t) = 0$, and with $Cv \gg R$, we obtain

$$\Psi_{ss} = C\left(1 + \frac{vx}{uh}\right) \qquad (5)$$

where we have assumed that $\Psi_{ss} = C$ at $x = 0$.

Next, we examine the behavior of the system after a step change in the flow rate. After a step change in velocity from u_0 to u_1, the concentration of cells near the surface evolves from one steady state to the next according to Eq. 4 with $u = u_1$:

$$\frac{\partial \Psi}{\partial t} = \frac{Cv}{h} - u_1 \frac{\partial \Psi}{\partial x}. \tag{6}$$

The general solution to this equation is

$$\Psi = \frac{Cv}{h} \tau + f(x - u_1\tau) \tag{7}$$

where $\tau = t - t_0$, the time since the step change occurred. The boundary and initial conditions, which determine the form of the function $f(x - u_1\tau)$, are that at $x = 0$, $\Psi = C$ (the bulk cell concentration), and at $\tau = 0$, the concentration must be equal to the previous steady-state value, $\Psi_{0,ss}$. These conditions lead to the following form of the function $f(x - u_1\tau)$, which has a discontinuous gradient at $x = u_1\tau$:

$$f(x - u_1\tau) = \begin{cases} C\left[1 + \dfrac{Cv}{u_1 h}(x - u_1\tau)\right] & x - u_1\tau \le 0 \\[3mm] C\left[1 + \dfrac{v}{u_0 h}(x - u_1\tau)\right] & x - u_1\tau > 0. \end{cases} \tag{8}$$

Substituting Eq. 8 into Eq. 7, we obtain the solution for the approach to the new steady state $(x > u_1\tau)$ and the new steady-state concentration profile $(x \le u_1\tau)$:

$$\Psi = \begin{cases} C\left(1 + \dfrac{vx}{u_1 h}\right) & x - u_1\tau \le 0 \\[3mm] \dfrac{Cv\tau}{h}\left(1 - \dfrac{u_1}{u_0}\right) + C\left(1 + \dfrac{vx}{u_0 h}\right) & x - u_1\tau > 0 \end{cases} \tag{9}$$

The time to reach steady state is $\Delta t_{ss} = x/u_1$, corresponding to the time required for a cell to move from $x = 0$ to the given x coordinate.

RESULTS AND DISCUSSION

We confirmed our assumptions regarding the velocities by examining cells that can be distinguished under experimental conditions at various flow rates, where the depth of field of the optical system is 13 μm. If the assumptions are correct, then the theoretical cell velocities at 13 μm and 20 nm should define the maximum and minimum limits, respectively, of the experimental velocities. 20 nm was chosen as the minimum distance because this is on the order of the bond interaction length: distances less than this should result in an interaction between the cell and surface (Bell, 1978). As Fig. 4 shows, the experimental velocities fall into the predicted range, and the experimental and theoretical mean velocities show good agreement.

The steady-state predictions of the model (Eq. 5) simulate the behavior of the system well. In Fig. 5, The concentration
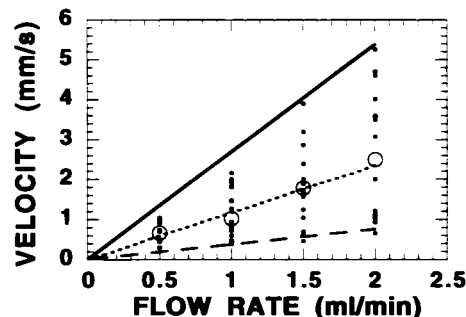

FIGURE 4   Verification of theoretical velocities. The velocities of randomly chosen cells were determined under experimental conditions over glass slides with no monolayer present at four different flow rates. The theoretical velocities at heights of 13 μm (———) and 20 nm (– – –) define the theoretical upper and lower velocity limits. The dotted line is the theoretical average velocity within h and the large circles are the experimental averages. The small circles are the sampled values at each flow rate.
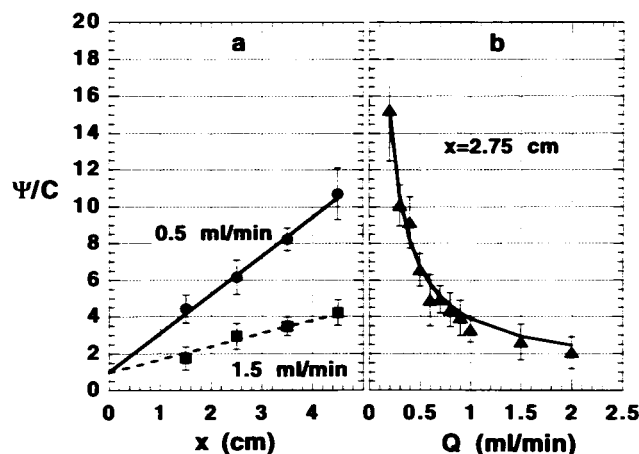

FIGURE 5   Steady-state cell concentrations within the layer h. T lymphocytes were perfused over a clean glass slide at various flow rates. After sufficient time had passed to reach steady state (see text), the cell concentration within h was determined at different x coordinates along the chamber. Panel a shows the linear relationship between the relative cell concentration and x for two different flow rates: 0.5 ml/min (theory: ———; experiment: ●; $r^2 = 0.992$) and 1.5 ml/min (theory: – – – –; experiment: ■; $r^2 = 0.959$). Panel b shows the comparison between theory (———) and experiment (▲) for Q at constant x ($x = 2.75$ cm). Error bars represent ± 1 SD from the mean of five measurements.

within h relative to the bulk concentration is plotted for various flow rates and distances along the chamber. The dependencies of concentration on x and Q are shown in Fig. 5, a and b, respectively. Note that there are no adjustable parameters in the model.

Fig. 6 illustrates a priori normalization of cell capture data through equalization of the cell fluxes during an experiment. The step changes in the flow rate are shown in Fig. 6 a and the resulting relative concentration, Ψ/C, in Fig. 6 b. The corresponding flux at the surface is plotted in Fig. 6 c. The flux and the rate of return to steady state are inversely proportional to the flow rate (Eq. 9), and the saw-tooth pattern of the flux is a result of the immediate decrease in the velocity
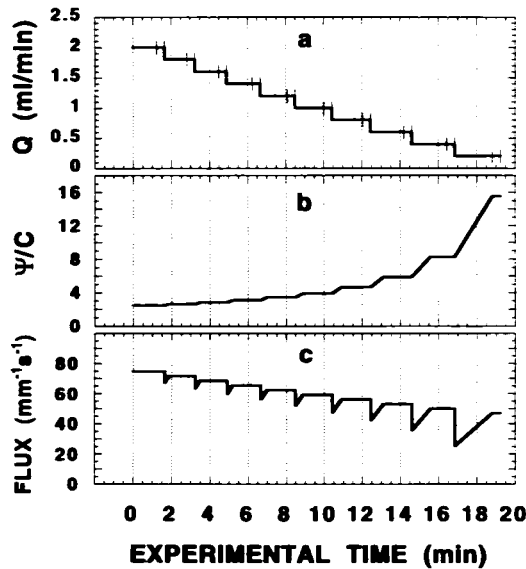
FIGURE 6 Normalization of cell fluxes during a cell capture experiment. Panel a shows the experimental steps in the flow rate; sampling was performed during the last 25 s at steady state, as indicated by the vertical hatch marks in the flow rate plot. The resulting time-course of the cell concentration and the cell flux within h at the center of the chamber ($x = 2.75$ cm) are plotted in b and c, respectively.

FIGURE 7 T cell binding to a TNF-α-activated HUVEC monolayer. The cumulative bound cell concentration (σ_b) is plotted as a function of the wall shear stress for an experiment using the protocol in Fig. 6. Error bars represent ±1 SD from the mean of five fields.

at the step changes followed by the approach to a new steady state of Ψ. During this period, the increase in concentration at the surface partially compensates for the decrease in velocity. By adjusting the waiting period at each flow rate, the areas under the flux curve in Fig. 6 c have been equalized for each step. The waiting period at 0.2 ml/min was first chosen so that Ψ just reaches steady state before sampling commences. The remaining flow times were calculated by equalizing the total number of cells, G_i, passing at each step according to

$$G_i = \frac{Cx}{2}\left(\frac{u_{i-1}}{u_i} + \frac{2vx}{u_ih} + 1\right)$$
$$+ Cu_i\left(1 + \frac{vx}{u_ih}\right)\left(t_{wi} - \frac{x}{u_i}\right)$$

(10)

where u_i and u_{i-1} are the current and previous velocities, respectively, and t_{wi} is the time spent at flow rate i (including sampling time).

Fig. 7 shows the resulting cumulative bound cell density as a function of shear stress for the protocol in Fig. 6. The bound cell density rises steadily after a transition period at the beginning. This transition region near 3 dyn/cm² represents the "critical capture stress" referred to by some authors (Mege et al., 1986; Lawrence and Springer, 1991; Menter et al., 1992), and at lower shear stresses (lower flow rates) the binding efficiency rises steadily. The value of the critical shear stress obtained using this technique agrees well with reports from other groups investigating a variety of cell types from polymorphonuclear leukocytes (Lawrence and McIntire, 1987) to sickle cells (Barabino et al., 1987), indicating that this is a robust parameter.
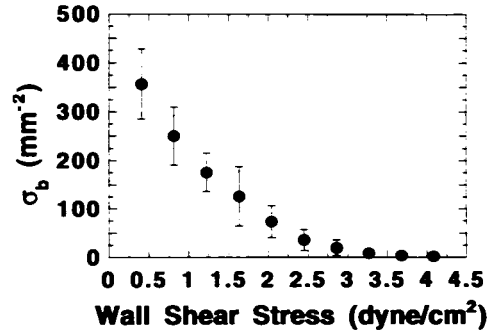
Various adhesion molecules can contribute to the net adhesive force to different degrees and at different times during the process of initial contact and arrest. The critical attachment thresholds as well as the different binding efficiencies (which are proportional to the slope of the binding curve) might prove to be useful indicators of the relative contribution of different molecular adhesion systems in mediating the early steps of cell binding under flow conditions. This hypothesis might be tested, for example, by performing antibody blocking experiments to eliminate the known adhesion systems one at a time.

These points are contingent, however, upon the normalization of the total number of cells available for binding over the course of the experiment. Without appropriate control of the cell fluxes, it is difficult to deduce the intrinsic binding kinetics from the experimental curves. The protocol outlined in Fig. 6 varies t_{wi} to equalize the number of cells at each flow rate. A protocol that uses equal waiting periods at each flow rate, on the other hand, results in a 51% decrease in the number of cells at the last step compared with the first. The decrease in the number of cells in this case is caused by the decrease in total flux as the flow rate decreases and as the system deviates from steady state. Binding data derived from such a protocol can be misleading because of the varying number of cells available for binding at each flow rate.

We must note that the current model represents a first-order correction that enables more reliable estimates of cell binding efficiencies, and correspondingly carries some limitations resulting from the assumptions that might restrict its application. One possible problem lies in the assumption of a universal and constant sedimentation velocity for the cells in the region above h. The cell flux predicted by the model is directly proportional to this sedimentation velocity, which in turn depends on the difference between the cell density and the fluid density, $\rho_s - \rho_L$. The range of lymphocyte density is 1.055 to 1.070, with mean 1.063 g/cm³ (Skalak and Chien, 1987). This corresponds to a ±12% range of sedimentation velocities around the mean, indicating that the population of cells at the bottom of the chamber will be enriched with cells of higher density. The experimental protocol could be improved, therefore, by using cells that have been previously

isolated over a tighter range of density. It should be noted, however, that the enrichment of cells of higher density only becomes a problem if the cell density carries some correlation with cell subtype or function. If density does not relate to cell adhesivity, or if we are not preferentially capturing one cell subset, then any density variation in the captured population would be acceptable for adhesion studies.

In addition, the assumption that $Cv \gg R$ might not hold in certain experimental protocols. This situation can occur, for example, in the adhesion of cells to a reactive surface or an endothelial monolayer, if there exists a large area for adhesion between the inlet and the point of observation. In these cases, the rate of binding can be comparable with the rate of supply from the bulk, and the steady-state concentration near the surface takes the form

$$\Psi_{ss} = \left(\frac{Cv - R}{uh}\right)x + C \tag{11}$$

Based on our experiments with lymphocytes binding to activated endothelial cells, the maximum rate of binding (corresponding to the lowest shear stress considered, 0.41 ml/min) is approximately 80 cells·cm^{-2}·s^{-1}. The sedimentation flux, on the other hand, is approximately 180 cells·cm^{-2}·s^{-1}. In this case, the assumption that $Cv \gg R$ is not valid. We circumvent this problem by seeding the HUVEC cells at the center of the slide, so that they cover only 1 cm^2 of the slide surface. This minimizes the region in which R is important and also allows us to conserve endothelial cells. The effect of depletion in the region upstream from the point of interest, therefore, is minimized. The steady-state concentration at the surface in this case is

$$\Psi'_{ss} = \frac{Cvx - R(x - x_0)}{uh} \tag{12}$$

where x_0 is the value of x at which the layer begins. For observations at the center of this 1 cm^2 region (at $x = 2.75$ cm), the reduction in cell concentration caused by binding is only 5% in the worst case (i.e., the lowest flow rate). For the situation where the entire surface is reactive and R cannot be neglected, the analysis is still valid, but cannot be used to define an a priori normalization. However, the theory could be applied to the resulting data to normalize with respect to the cell flux after determining the rates of binding in the above equation.

The presented analysis has important ramifications for flow chamber studies in general. First, this study has shown that there are variations in fluxes along the chamber length; therefore, any assessment of cell capture in the flow chamber must either maintain a constant x coordinate or else correct for the differences in flux because of sampling along the chamber. Second, the steady-state value of the flux depends on the flow rate, and studies comparing different wall shear stresses by adjusting the flow rate must account for these differences. Even devices that have been designed to provide a varying shear rate without necessitating flow rate changes, such as the radial flow chamber (Groves and Riley, 1987; Kuo and Lauffenburger, 1993) and the parallel plate flow

chamber with variable width (Usami et al., 1993), must apply similar corrections for cell delivery. Finally, the temporal nature of the flux after a step change in the flow rate must be considered, because this leads to additional variations in the rate of cell delivery to the surface.

The purpose of this analysis was to develop a more accurate method for obtaining and interpreting binding data for cell capture in the parallel plate flow chamber. It provides an estimate of the cell concentration near the surface, which should be related to the collision frequency between cells and the surface. The theory is consistent with the experimental observations and represents an improvement over simpler techniques that normalize the bound cell density with respect to the flux based on the bulk cell concentration. It is a first step toward a more detailed analysis that would model the physical interaction between the cell and surface as well as the kinetics of receptor-ligand binding, and thereby relate binding rates to molecular adhesion mechanisms.

REFERENCES

Abassi, O., C. L. Lane, S. Krater, T. K. Kishimoto, D. C. Anderson, L. V. McIntire, and C. W. Smith. 1991. Canine neutrophil margination mediated by Lectin Adhesion Molecule-1 in vitro. J. Immunol. 147: 2107–2115.

Barabino, G. A., L. V. McIntire, S. G. Eskin, D. A. Sears, and M. Udden. 1987. Endothelial cell interactions with sickle cell trait, mechanically injured, and normal erythrocytes under controlled flow. Blood. 70: 152–157.

Bell, G. I. 1978. Models for the specific adhesion of cells to cells. Science. 200:618–627.

Brenner, H. 1961. The slow motion of a sphere through a viscous fluid towards a plane surface. Chem. Eng. Sci. 16:242–251.

Doroszewski, J., Z. Golab-Meyer, and W. Guryn. 1979. Adhesion of cells in flowing suspensions: effects of shearing force and cell kinetic energy. Microvasc. Res. 18:421–433.

Forrester, J. V., and J. M. Lackie. 1984. Adhesion of neutrophil leucocytes under conditions of flow. J. Cell Sci. 70:93–110.

Gallik, S., S. Usami, K.-M. Jan, and S. Chien. 1989. Shear stress-induced detachment of human polymorphonuclear leukocytes from endothelial cell monolayers. Biorheology. 26:823–834.

Goldman, A. J., R. G. Cox, and H. Brenner. 1967. Slow viscous motion of a sphere parallel to a plane wall-II. Couette flow. Chem. Eng. Sci. 22: 653–660.

Groves, B. J., and P. A. Riley. 1987. A miniaturised parallel-plate shearing apparatus for the measurement of cell adhesion. Cytobios. 52: 49–62.

Hochmuth, R. M., N. Mohandas, E. E. Spaeth, J. R. Williamson, P. L. Blackshear, Jr., and D. W. Johnson. 1972. Surface adhesion, deformation and detachment at low shear of red cells and white cells. Trans. Am. Soc. Artif. Organs. 18:325–332.

Kuo, S. C., and D. A. Lauffenburger. 1993. Relationship between receptor/ligand binding affinity and adhesion strength. Biophys. J. 65:2191–2200.

Lawrence, M. B., and L. V. McIntire. 1987. Effect of flow on polymorphonuclear leukocyte/endothelial cell interactions. Blood. 70:1284–1290.

Lawrence, M. B., and T. A. Springer. 1991. Leukocytes roll on a selectin at physiological flow rates: distinction from and prerequisite for adhesion through integrins. Cell. 65:859–873.

Leung, K. H. 1989. Human lymphokine-activated killer (LAK) cells I. Depletion of monocytes from peripheral blood mononuclear cells by L-phenylalanine methyl ester and optimization of LAK cell generation at high density. *Cancer Immunol. Immunother.* 30:247–254.

Mege, J. L., C. Capo, A. M. Benoliel, and P. Bongrand. 1986. Determination of binding strength and kinetics of binding initiation. *Cell Biophys.* 8: 141–160.

Menter, D. G., J. T. Patton, T. V. Updyke, R. S. Kerbel, M. Maamer, L. V. McIntire, and G. L. Nicolson. 1992. Transglutaminase stabilizes melanoma adhesion under laminar flow. *Cell Biophys.* 18:123–143.

Skalak, R., and S. Chien. 1987. Handbook of Bioengineering. McGraw-Hill, New York. 31.

Usami, S., H. Chen, Y. Zhao, S. Chien, and R. Skalak. 1993. Design and construction of a linear shear stress flow chamber. *Ann. Biomed. Eng.* 21:77–83.

van Kooten, T. G., J. M. Schakenraad, H. C. van der Mei, and H. J. Busscher. 1992. Development and use of a parallel-plate flow chamber for studying cellular adhesion to solid surfaces. *J. Biomed. Mat. Res.* 26:725–738.

Wattenbarger, M. R., D. J. Graves, and D. A. Lauffenburger. 1990. Specific adhesion of glycophorin liposomes to a lectin surface in shear flow. *Biophys. J.* 57:765–777.

Yaumachi, A., and E. T. Bloom. 1993. Requirement of thiol compounds as reducing agents for IL-2 mediated induction of LAK activity and proliferation of human NK cells. *J. Immunol.* 151:5535–5544.